Investigation on switchable operation states in a Tm/Ho co-doped fiber laser based on nonlinear optical loop mirror*

WANG Xiaofa, PAN Jiamin, and HE Yiping**

School of Optoelectronic Engineering, Chongqing University of Posts and Telecommunications, Chongqing 400065, China

(Received 4 December 2022; Revised 4 February 2023)

The nonlinear pulse dynamics have been studied in a thulium/holmium co-doped passively mode-locked fiber laser based on nonlinear optical loop mirror (NOLM). By enhancing the nonlinear effect of the cavity and without changing the polarization state of the cavity, four types of operation states that switch between each other, including the basic mode-locking pulse, the two solitons pulse, the bright-dark pulse, and the harmonic mode-locking pulse, can be obtained. Compared with the laser of single mode-locking state, passively mode-locked fiber lasers (PMLFLs) with switchable operation states can be used in a wide range of applications, such as optical communication, material processing and optical fiber sensing technology.

Document code: A **Article ID:** 1673-1905(2023)08-0455-7

DOI https://doi.org/10.1007/s11801-023-2206-y

Passively mode-locked fiber lasers (PMLFLs) are widely used in the fields of medicine, material processing, lidar and optical communication[1] due to their advantages, such as good beam quality, low threshold, easy operation, long life and low cost[2]. PMLFLs with different saturable absorbers (SAs) for mode-locking can output the complex pulse dynamics, such as conventional soliton[3], multiple solitons pulse[4], dissipative soliton resonance (DSR)[5], bright-dark pulse (BDP)[6], harmonic mode-locking (HML) pulse[7] and noise like pulse (NLP)[8], etc. Therefore, PMLFLs can be used as an ideal platform to study nonlinear dynamic characteristics in laser systems.

As a key component of PMLFLs, SA can be divided into real SAs and artificial SAs. Real SAs include semiconductor saturable absorber mirror[9], carbon nanotubes[10] and graphene[11], etc. And artificial SAs include nonlinear polarization rotation (NPR)[12], nonlinear optical loop mirror (NOLM)[13] and nonlinear amplifying loop mirror (NALM)[14]. Compared with real SAs, artificial SAs have the advantages of simple structure, low cost, high damage threshold and high integration[15], and have been widely covered 1—2 μm band PMLFLs[16]. Among artificial SAs, NOLM has been widely studied by scholars in recent years due to its advantages of high environmental stability, short response time and low polarization dependence[17]. In the 1—2 μm band, basic mode-locking (BML) pulse[18], DSR pulse[19], and NLP[20] have been obtained by optimizing the pump power and polarization state in PMLFLs based on NOLM.

Despite one type of mode-locking state can be generated by PMLFLs, it is difficult to meet the requirements of practical application requiring switchable mode-locking operations. So, scholars have sought some solutions in recent years. In 2022, WU et al[21] obtained the bright pulse, multi-pulse and soliton molecules in erbium-doped fiber laser based on NALM by adjusting pump power and polarization controller (PC), respectively. In 2022, PAUL et al[22] built ytterbium-doped fiber laser based on NOLM, and simultaneously obtained rectangular dark pulses and bright pulses by changing the pump power and intracavity polarization state. In the same year, PAN et al[23] obtained NLP and DSR pulses in ytterbium-doped fiber laser with NOLM structure by adjusting PC. In a recent study, LI et al[24] obtained comb soliton beams, conventional soliton and NLP in an erbium-doped fiber laser based on NOLM by optimizing pump power and intracavity polarization states. However, the above laser can only produce two or three types of switchable states in the process of increasing the pump power, and the switching between different mode-locking states can only be realized by adjusting the PC to a suitable state, which is not convenient for application.

Compared with ytterbium-doped gain fiber in 1 μm band and erbium-doped gain fiber in 1.5 μm band, thulium-holmium co-doped gain fiber in 2 μm band has a wider emission spectrum, so the mode competition effect is more pronounced and may generate more nonlinear

* This work has been supported by the Natural Science Foundation of Chongqing City (No.CSTC2018jcyjAX0585).

** E-mail: wangxf@cqupt.edu.cn

dynamic states of pulse. In this paper, an experimental configuration about the thulium/holmium co-doped mode-locked fiber laser (THDFL) based on NOLM was proposed. Without changing intracavity polarization state, different switchable operation states can be obtained in THDFL by increasing the pump power, which are continuous wave (CW), BML pulse, two solitons mode-locking (TSML) pulse, BDP, transition region (TR) and HML pulse, respectively. The PMLFLs with switchable operation states not only have more application spaces than the ordinary laser, also can provide the reference for studying the nonlinear dynamic characteristics of PMLFLs.

The experimental setup is schematically shown in Fig.1. The configuration adopts a 1 550/1 950 nm wavelength division multiplexer (WDM) to introduce the pump light emitted by the 1 550 nm semiconductor laser into the resonator. The 30/70 optical coupler (OC1) is used to split the light, of which 30% laser is used as the output light, and 70% is feedback. A 10/90 OC2 is used to connect the unidirectional and bidirectional rings of the resonator. A polarization independent isolator (PI-ISO) is utilized to ensure the unidirectional operation. PC1 and PC2 are used to fine-tune and coarsely adjust the linear phase bias to achieve a stable mode-locking output. The total length of the resonator is about 116 m, including a 2.5-m-long thulium/holmium co-doped fiber (THDF, TH512) as a gain medium, with an absorption coefficient of 13.3 dB/m at 1 550 nm, the fiber core/cladding diameters of 9/125 μm, and the numerical aperture is 0.16; approximately 13.5 m device pigtail (SMF28e); highly nonlinear fiber (HNLF, 1 550-Zero) of 100 m. The nonlinear effect can be enhanced by adding HNLF with a nonlinear coefficient of about 10 $(W\cdot km)^{-1}$ to the resonator cavity. In the experiment, the spectrum is monitored by a spectral analyzer (Omni-λ750i, Zolix) with a resolution of 0.05 nm. The pulse waveform and radio frequency (RF) spectra are measured by InGaAs photodetector (ET-5000F, EOT) connected to digital oscilloscope (WaveRunner 610Zi, Lecroy) with bandwidth of 1 GHz and RF analyzer (FSL3, Rohde & Schwarz) with a bandwidth of 3 GHz, respectively.

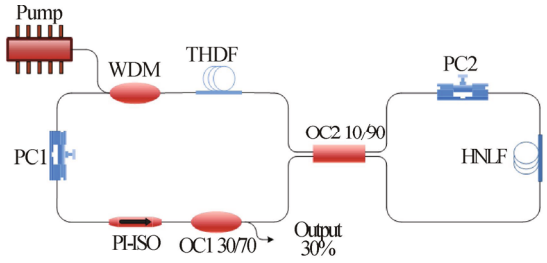

Fig.1 Experimental setup of the thulium/holmium co-doped mode-locked fiber laser

In order to explore the nonlinear dynamic characteristics in THDFL, the average output power under different pump powers are experimentally measured, as shown in Fig.2. The average output power increases linearly with the pump power. The threshold of continuous wave is 0.39 W. When the pump power increases from 0.39 W to 1 W, THDFL shows six types of operation states after reaching the oscillation threshold, including CW (0.39—0.49 W), BML (0.49—0.52 W), TSML (0.52—0.62 W), BDP (0.62—0.82 W), TR (0.82—0.90 W), and HML (0.90—1 W). In addition, when the maximum pump power is 1 W, the average output power is 38.70 mW, and the slope efficiency of THDFL in the experiment is ~6.30%. The main reason for the low slope efficiency is due to the mode field mismatch between the double-clad THDF and the WDM fiber pigtails, and the large loss of HNLF in the 2 μm band.

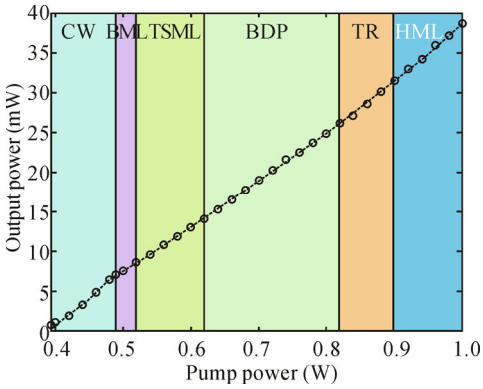

Fig.2 Average output power under different pump powers

When the pump power increases to 0.49 W, the laser reaches the mode-locking threshold. By carefully adjusting the PC, the BML pulse is obtained. Fig.3 shows the corresponding mode-locking oscilloscope trace, optical spectrum, and RF spectrum, respectively. The time series of the BML pulse is shown in Fig.3(a), whose pulse width is 1.47 ns. The insert shows the time interval between adjacent pulses in the pulse sequence is 626.70 ns, and its corresponding repetition rate is 1.59 MHz. Fig.3(b) shows the fitting autocorrelation trace of the BML pulses. In order to study the stability of the laser, the RF spectrum in the range of 200 MHz is measured at the resolution bandwidth (RBW) of 1 kHz, as shown in Fig.3(c). The spectrum of the laser is flat and there is no modulation. It shows that the laser has good mode-locking stability. The detection results of spectrum are shown in Fig.3(d). As can be seen from the figure, the center wavelength of the BML pulse is located near 1 916.9 nm, and its full width at half maximum (*FWHM*) is about 5.8 nm. Moreover, it can be observed that the spectrum has a significant decrease at 1 921 nm. This is caused by the absorption of the 2 μm band laser by water molecules and carbon dioxide.

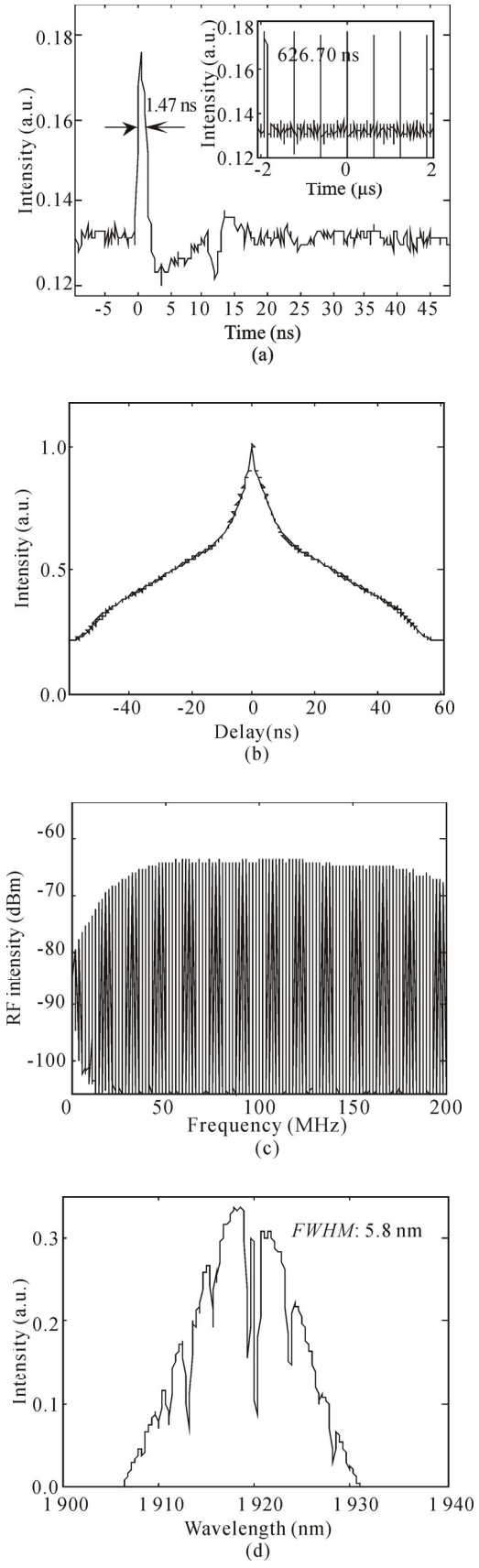

Fig.3 Output characteristics of the BML pulse: (a) Oscilloscope trace (Insert: the corresponding pulse trains); (b) Autocorrelation trace; (c) The RF spectrum with a span range of 200 MHz; (d) Optical spectrum

When the pump power is increased to 0.52 W, the pulse splitting can be observed. The stable BML operating state of the laser is broken, and THDFL enters a state of the TSML operating. It is worth noting that TSML is very common in fiber lasers, which is caused by excessive accumulation of nonlinear phase shifts in the cavity and peak clamping effect[25]. Fig.4 depicted the output characteristics of the two solitons state. Compared with the bright pulse, the TSML has two pulses, and the period of round-trip is constant. The single pulse of the two solitons is shown in Fig.4(a). It can be seen that the pulse width of the TSML is 1.80 ns. It can be seen that the time interval between the two solitons is 20.80 ns, and the corresponding frequency is 48 MHz. While increasing the pump power, the time interval of the two pulses of the TSML remains stable. The intensity of the two pulses of the TSML is basically the same, but there is a small amplitude fluctuation, which may be caused by the gain competition between the two solitons and the experimental environment noise, such as the vibration of optical fiber and air turbulence[26]. It can be seen from the insert that the time interval of the pulse train is 626.70 ns, and the corresponding repetition rate is 1.59 MHz. Fig.4(b) shows the fitting autocorrelation trace of the TSML pulses. In order to further explore the output characteristics of the TSML, the corresponding RF spectrum is also observed, and the spectrum diagram is shown in Fig.4(c). Interestingly, it can be clearly found that there is an obvious envelope modulation phenomenon in the spectrum, whose modulation frequency is just equal to the reciprocal of the time interval between the two solitons, and similar reports have been reported in Ref.[27]. The spectrogram of the two solitons is shown in Fig.4(d). Its center wavelength is 1 917.8 nm and *FWHM* is 5.9 nm.

Then, we focus on the output characteristics of BDPs when the pump power is 0.62 W, as shown in Fig.5. It can be clearly seen from Fig.5(a) that the pulse widths of bright and dark pulses are 2.20 ns and 3.00 ns, respectively. The time interval between bright and dark pulses is about 10.00 ns. When the pump power increases from 0.62 W to 0.82 W, the pulse width of the bright pulse and the dark pulse basically remain unchanged. In a uniform continuous wave background, the intensity of the dark pulse is slightly lower than that of the bright pulse. A low intensity bright pulse is found on the right side of the dark pulse, which is similar to the bright-dark-bright pulse in Ref.[28]. The weak bright pulse may be the result of the echo signal of electron recovery in the photodiode detector[29]. It can be seen from the insert that the time interval between adjacent pulses is 626.70 ns, and the corresponding repetition rate is 1.59 MHz. Fig.5(b) shows the fitting autocorrelation trace of the BDP pulses. The RF spectrum with a resolution bandwidth of 1 kHz and a span of 200 MHz is shown in Fig.5(c). There is an obvious envelope modulation phenomenon, which is the same as spectrum of TSML operation. And the corresponding modulation frequency is approximately equal to the reciprocal of

the time interval between the bright pulse and the dark pulse. Fig.5(d) shows the center wavelength of the BDP is 1 921.6 nm, and the *FWHM* is 7.6 nm.

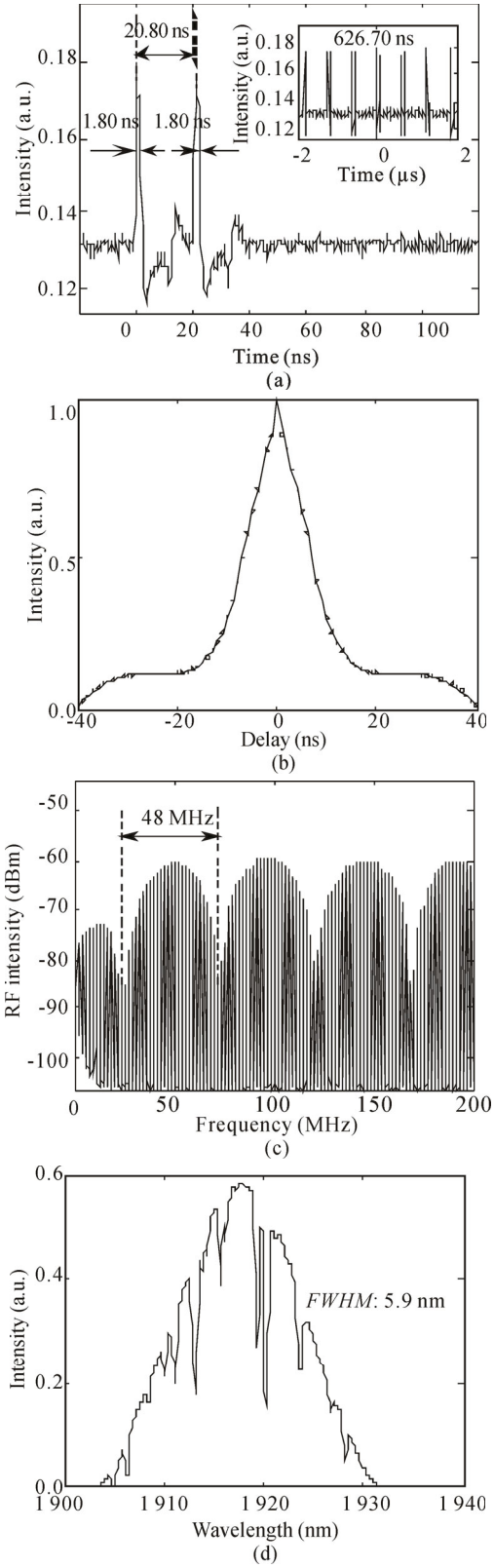

Fig.4 Output characteristics of the TSML pulse: (a) Oscilloscope trace (Insert: the corresponding pulse trains); (b) Autocorrelation trace; (c) The RF spectrum with a span range of 200 MHz; (d) Optical spectrum

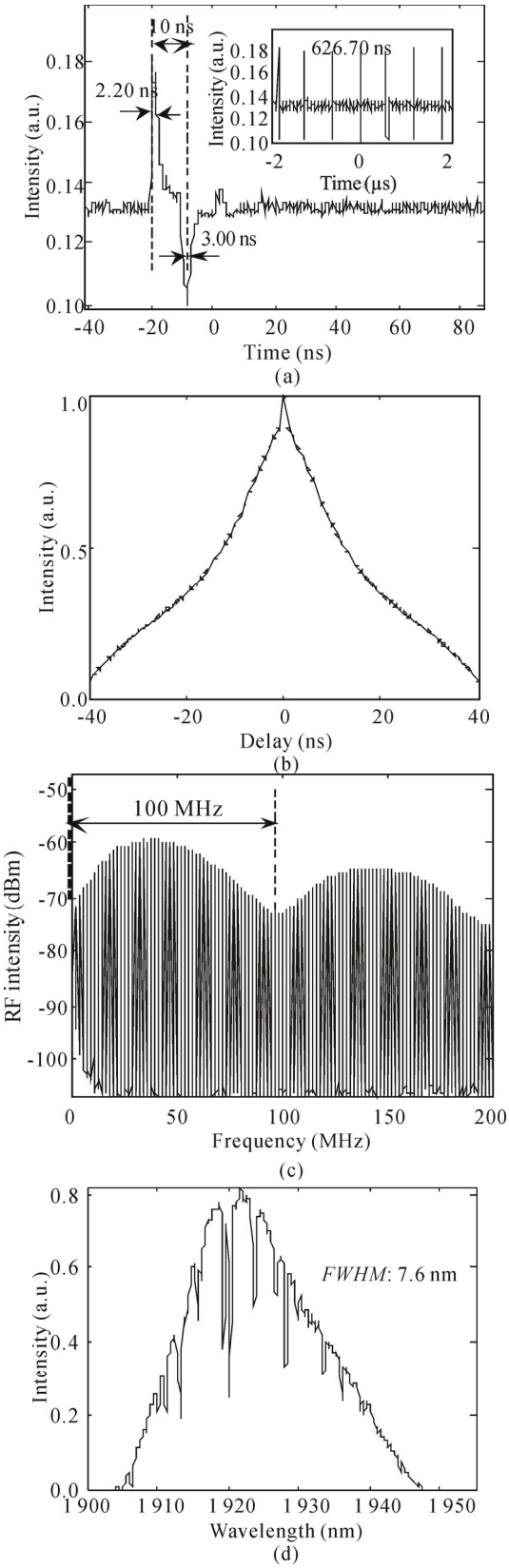

Fig.5 Output characteristics of the BDP: (a) Oscilloscope trace (Insert: the corresponding pulse trains); (b) Autocorrelation trace; (c) The RF spectrum with a span range of 200 MHz; (d) Optical spectrum

When the pump power is between 0.82 W and 0.90 W,

the laser turns into the transition region. The pulse amplitude fluctuates significantly, and the frequency is no longer stable at 1.59 MHz, which may be caused by environmental disturbance, interaction between solitons and the existence of dispersive waves[30]. However, when the pump power level exceeds the 0.90 W value, the pulse with obvious amplitude fluctuation becomes a stable second-order HML pulse[31]. And the order of harmonics remains unchanged in the process of increasing the pump power from 0.9 W to 1 W. The HML can be explained by the quantization theory of soliton energy. The intrinsic optical pulse energy of the soliton does not increase with pump power, which leads to multi-pulse oscillation in the resonator. In addition, there is mutual repulsion between solitons, so multiple pulses can form a special state of equally spaced pulses in the laser cavity, namely HML. Fig.6 shows the output characteristics of the HML pulse. The oscilloscope trace of the HML pulse is shown in Fig.6(a), and its pulse width is 3.60 ns. The inset of Fig.6(a) shows that the time interval of adjacent pulses is 313.70 ns, and the corresponding repetition rate is 3.19 MHz. The fitting autocorrelation trace of the BDP pulses is shown in Fig.6(b). When the pump power is increased to 1 W, the spectrum stability of the laser is tested. Fig.6(c) shows that the signal to noise ratio of the laser is ~42 dB, and the harmonic RF peak is located at 3.19 MHz, indicating that the mode-locking pulse works in a stable state. The inset in Fig.6(c) shows the spectrum under the span of 200 MHz. It can be seen that there is no modulation phenomenon in the spectrum. It can be seen from Fig.6(d) that the *FWHM* of the HML spectrum is 22.6 nm, and the central wavelength is 1 931.5 nm. Compared with the central wavelength of mode-locking pulse of the fundamental frequency, the central wavelength of HML spectrum has red shift. And the spectrum has obvious broadening phenomenon.

In this paper, a thulium-holmium co-doped passively mode-locked fiber laser based on an NOLM is constructed. The nonlinear effect of the resonator cavity is enhanced by adding a 100-m-long HNLF to a bidirectional ring. By optimizing the pump power and intracavity polarization state, four types of different mode-locking states are experimentally obtained, including BML pulse, TSML

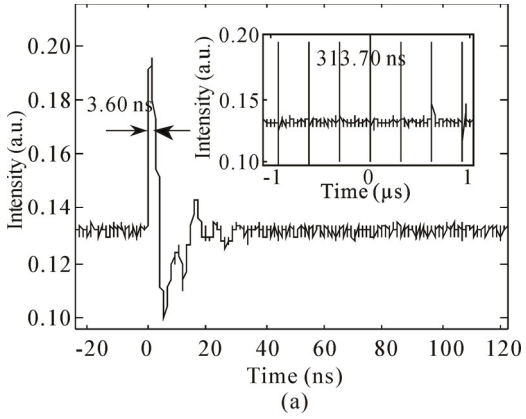

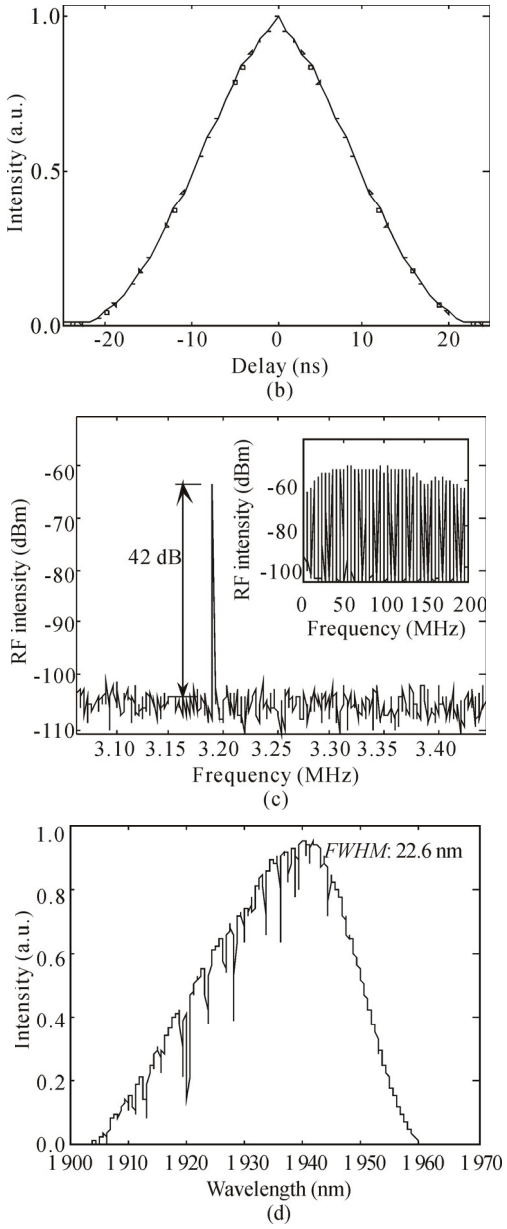

Fig.6 Output characteristics of the HML pulse: (a) Oscilloscope trace (Insert: the corresponding pulse trains); (b) Autocorrelation trace; (c) The RF spectrum (Insert: RF spectrum with a span range of 200 MHz); (d) Optical spectrum

pulse, BDP and HML pulses. The TSML pulse and BDP have obvious envelope modulation phenomenon on the corresponding RF spectrum, and their modulation frequencies are approximately the reciprocal of the two solitons interval and the bright and dark pulse interval, respectively. At the maximum pump power of 1 W, the output power of THDFL, center wavelength, and *FWHM* are 38.70 mW, 1 931.5 nm, 22.6 nm, respectively. In addition, when the laser reaches the mode-locking threshold, multiple switchable mode-locking states can be obtained without adjusting the PC. The results provide the experimental reference for further study of the switching between different states and the nonlinear

dynamic characteristics of multiple solitons pulse, BDP and HML pulse in PMLFLs.

Ethics declarations

Conflicts of interest

The authors declare no conflict of interest.

References

[1] RUDY C W, DIGONNET M J F, BYER R L. Advances in 2-μm Tm-doped mode-locked fiber lasers[J]. Optical fiber technology, 2014, 20(6)：642-649.

[2] MAJEWSKI M R, JACKSON S D. Highly efficient mid-infrared dysprosium fiber laser[J]. Optics letters, 2016, 41(10)：2173-2176.

[3] YANG F, SUN S, CHEN S, et al. Passively mode-locked Er-doped fiber laser based on a ferromagnetic insulator $Cr_2Si_2Te_6$ as a saturable absorber[J]. Applied optics, 2022, 61(4)：898-903.

[4] WANG S F, WANG D N, XIA Q K, et al. Multi-soliton pulse generation in a fiber laser by using a long-period fiber grating[J]. International journal for light and electron optics, 2022, 270：170017.

[5] WU Y F, DONG Z K, HUA L L, et al. Improvement of peak power of dissipative soliton resonance pulse in a thulium-doped fiber laser[J]. Optics and laser technology, 2023, 157：108656.

[6] WANG X F, LIU D X, HAN H H, et al. Generation of cavity-birefringence-dependent multi-wavelength bright-dark pulse pair in a figure-eight thulium-doped fiber laser[J]. Chinese physics B, 2021, 30(05)：276-280.

[7] YANG S, ZHENG J C, QI Y Y, et al. Widely-tunable harmonic mode-locked fiber laser by the combination of spectral filtering and gain management[J]. Optics and laser technology, 2023, 157：108726.

[8] HUANG J J, SUN Y, XIE Y N, et al. Spectral dynamics of noise-like square pulses generated in a Tm-doped figure-8 fiber laser[J]. Optics and laser technology, 2022, 158：108595.

[9] TANG Y L, LI F, YU X C. Dual-wavelength harmonic mode-locked dissipative soliton resonance of Yb fiber laser[J]. Optics and laser technology, 2022, 152：108147.

[10] ZHU Y X, ZENG C, HE Z W, et al. Ultrafast all-anomalous-dispersion Er-doped large-mode-area fiber lasers[J]. Optics and laser technology, 2022, 148：107783.

[11] WANG X F, ZHANG J H, PENG X L, et al. Generation and evolution of multiple operation states in passively mode-locked thulium-doped fiber laser by using a graphene-covered-microfiber[J]. Chinese physics B, 2018, 27(08)：305-311.

[12] HU P, MAO J J, ZHOU X, et al. Passively mode-locked Ho-doped fiber laser with soliton rain and noise-like pulse regime[J]. Optics and laser technology, 2022, 153：108215.

[13] GUO Y, YAN F P, QIN Q, et al. Wavelength-interval-switchable multi-wavelength thulium-doped fiber laser with a nonlinear dual-pass Mach-Zehnder interferometer filter in 2-μm-band[J]. Optics and laser technology, 2022, 145：107470.

[14] TAO J N, SONG Y Q, LI Y Y, et al. Pulse type switchable, spectral bandwidth dynamically adjustable all-fiber laser mode-locked by NALM[J]. Optics and laser technology, 2022, 145：108682.

[15] WANG Z H, ZHANG B, LIU J, et al. Recent developments in mid-infrared fiber lasers：Status and challenges[J]. Optics and laser technology, 2020, 132：106497.

[16] RUDY C W, URBANEK K E, DIGONNET M J, et al. Amplified 2-μm thulium-doped all-fiber mode-locked figure-eight laser[J]. Journal of lightwave technology, 2013, 31(11)：1809-1812.

[17] DONG Z K, SONG Y R. Research progress of mode-locked fiber lasers based on saturable absorbers[J]. Chinese journal of lasers, 2021, 48(5)：98-113.

[18] GUO Y X, LI P L, GUO P L, et al. Supercontinuum generation in an Er-doped figure-eight passively mode-locked fiber laser[J]. Optics express, 2018, 26(8)：9893-9900.

[19] LIU S M, ZHANG Z X, SHEN J P, et al. Wavelength-spacing adjustable dual-wavelength dissipative soliton resonance thulium-doped fiber laser[J]. IEEE photonics journal, 2019, 11(2)：1-9.

[20] WANG M, LIU M Q, CHEN Y W, et al. Stable noise-like pulse generation in all-PM mode-locked Tm-doped fiber laser based on NOLM[J]. Chinese optics letters, 2021, 19(9)：62-66.

[21] WU J W, LIU G X, GAO Y X, et al. Switchable femtosecond and picosecond spatiotemporal mode-locked fiber laser based on NALM and multimode interference filtering effects[J]. Optics and laser technology, 2022, 152：108414.

[22] PAUL C, SINGH C P, GUPTA P K, et al. Rectangular dark pulses in all-normal dispersion fiber oscillator[J]. Optics and laser technology, 2022, 147：107641.

[23] PAN Y Z, QIU H X, ZHANG T Q, et al. Dissipative soliton resonance and noise-like pulse generation of large normal dispersion Yb-doped fiber laser[J]. Optica applicata, 2022, 52(1)：77-88.

[24] LI M X, SHU Y Q, GU L, et al. Modulated comb-like pulse distribution induced by intracavity Sagnac filtering in a fiber laser[J]. Optics and laser technology, 2022, 145：107480.

[25] WANG G D, YANG G, LIU Y G, et al. Soliton bundles and high-order harmonic mode-locked in Tm-doped fiber laser[J]. Chinese journal of lasers, 2017, 44(8)：83-87.

[26] WU T, HUANG J Z, WANG M Y, et al. Generation of pulse bundles and bundle groups in a mode-locked Tm-doped fiber ring laser[J]. Journal of optoelectronics·laser, 2021,

32(2)：209-216. (in Chinese)

[27] WANG X D, YANG S M, SUN M Q, et al. Generation of multi-wavelength square pulses in the dissipative soliton resonance regime by a Yb-doped fiber laser[J]. Chinese physics B, 2020, 30(6)：390-395.

[28] WU Q C, WU Z, YAO Y, et al. Three-component bright-dark-bright vector pulse fiber laser based on MoS_2 saturable absorber[J]. Optics communications, 2021, 498：127231.

[29] CHERNYAK L, SCHULTE A, OSINSKY A, et al. Influence of electron injection on performance of GaN photodetectors[J]. Applied physics letters, 2002, 80(6)：926-928.

[30] LI H F, ZHANG S M, DU J, et al. Passively harmonic mode-locked fiber laser with controllable repetition rate based on a carbon nanotube saturable absorber[J]. Optics communications, 2011, 285(6)：1347-1351.

[31] YANG H, LI X P, QI M T, et al. $TaSe_2$ nanosheets for harmonic mode-locked fiber laser[J]. Optical fiber technology, 2022, 72：102956.